Cova F, Fasoli M, Moretti F, Chiodini N, Pauwels K, Auffray E, Lucchini M T, Bourret E, Veronese I, d'Ippolito E, Vedda A

Optical properties and radiation hardness of Pr-doped sol-gel silica: Influence of fiber drawing process

(2017) J. Lumin, vol. 192, p. 661-667

doi: 10.1016/j.jlumin.2017.07.045

Optical properties and radiation hardness of Pr-doped Sol-Gel silica: influence of fiber drawing process

Francesca Cova[a], Mauro Fasoli[a] *, Federico Moretti[a], Norberto Chiodini[a], Kristof Pauwels[b], Etiennette Auffray[c], Marco Toliman Lucchini[c], Edith Bourret[d], Ivan Veronese[e,f], Eduardo d'Ippolito[e], Anna Vedda[a]

[a] Department of Materials Science, University of Milano-Bicocca, Via Cozzi 55, 20125 Milano (Italy)
[b] Department of Physics, University of Milano-Bicocca, Piazza della Scienza 3, 20125 Milano (Italy)
[c] CERN, Route de Meyrin, 1211 Geneva 23 (Switzerland)
[d] Materials Science Division, Lawrence Berkeley National Laboratory, Berkeley, CA (USA)
[e] Department of Physics, University of Milano, Via Celoria 16, 20133 Milano (Italy)
[f] INFN, Unit of Milano, Via Celoria 16, 20133 Milano (Italy)

* Corresponding author at: Department of Materials Science, University of Milano-Bicocca, Via Cozzi 55, 20125 Milano (Italy)
E-mail address: mauro.fasoli@mater.unimib.it (Mauro Fasoli)

Abstract The optical emission from the 5d – 4f allowed transition of Pr^{3+} ions embedded in sol-gel silica is investigated for High Energy Physics applications requiring fast scintillating materials.

A complete and detailed characterization of the optical, scintillation and radiation hardness properties of Pr-doped silica is carried out employing different experimental techniques including steady-state and time-resolved photo-luminescence, radio- and thermo-luminescence, scintillation and optical absorption.

Optical absorption measurements, performed after X-ray irradiation sequences up to 1 kGy, evidence the formation of radiation-induced absorption bands related to point defects acting as color centers. Spontaneous partial recovery of the radiation-induced defects at room temperature, as well as after thermal treatments, is also disclosed.

Particular attention is paid to the comparison between bulk silica, both before and after a melting process, and fibers. The results reveal the presence of a lower concentration of optically active defects in melted glass. Such comparison highlights a role of the fiber drawing in modifying the glass defectiveness, consisting in the occurrence of a structural reorganization of the amorphous network during the process.

Keywords: Sol-Gel, Rare-Earths, Scintillating fibers, Radiation damage

1. Introduction

In recent years, the sol-gel technique was demonstrated to allow a good control, at a relatively low densification temperature, of rare earth (RE) ions incorporation and of their dispersion inside the glass matrix. The glass synthesis can be performed by using high purity precursors, reducing the level of unwanted impurities [1]. This latter factor is an essential feature for the radiation hardness of such materials. In principle, glass matrices can host luminescent activators in large amounts. However, at concentrations above 1 mol%, the formation of RE-rich clusters was detected. This phenomenon was found to affect the scintillation efficiency as well as the glass homogeneity [1-3].

Several studies demonstrated that RE-doped silica glasses prepared by sol-gel route are suitable materials for the realization of scintillating optical fiber sensors, opening their application perspectives for real time dosimetry in medical systems ([4] and references therein). Glass fibers could be applied also as wavelength shifters for the collection and transport of scintillation light in High Energy Physics (HEP) experiments [5]. Moreover, and in parallel with undoped fibers exploiting Cherenkov light [6], the use of RE-doped fibers as scintillators in HEP detectors has been recently proposed as active materials in a sampling SPACAL-like electromagnetic calorimeter [7, 8] or as the scintillating component in a dual-readout calorimeter [9, 10].

A fast response (average decay time below 40 ns) and an extremely good radiation hardness are crucial properties of the material for such application. Radiation tolerance strongly depends on the kind of experiment and on the position of the fibers in the detector with respect to the beam line. The most challenging requirement is expected in the High Luminosity Large Hadron Collider phase [11], in which the radiation induced absorption coefficient of the scintillator material should be kept below 1-2 m^{-1} even after doses of 300 kGy.

Praseodymium dopant can be considered as a suitable luminescent activator, because of its fast (a few tens of ns) 5d - 4f transition leading to an emission band in the UV spectral region [12, 13]. The properties of Pr^{3+} ions incorporated in various crystalline matrices have been extensively investigated. LuAG and YAG garnet compounds and ceramics, as well as admixtures of Y and Ga into LuAG garnet crystals [14-19] have been characterized. Scintillation of Pr^{3+} in aluminum perovskite compounds, such as YAP [20, 21] and in silicates [22] have also been reported. On the other hand, the luminescence and scintillation properties of SiO_2:Pr glass have been considered in few cases in view of scintillator or laser applications [12, 23, 24].

The present work is aimed at the investigation of the optical and scintillation properties of Pr-doped silica glasses under intense irradiation fields, delivering doses up to 1.3 kGy. A comparison between bulk preforms and residuals of the fiber drawing process is also carried out, in order to disclose the role of this process in the radiation hardness properties of RE-doped silica glasses.

2. Experimental Methods

Pr-doped silica glass with Pr concentration of 0.05 mol% was prepared by the sol-gel method using tetramethylorthosilicate (TMOS) and Pr(III) nitrate as precursors. Alcogels were obtained after gelation and subsequently dried in a thermostatic chamber for a few weeks. The obtained xerogels were densified up to 1225 °C, in order to obtain a Pr-doped preform with dimensions of 70 mm in length and 10 mm diameter.

The preform was then drawn into fiber by Polymicro Technologies (Phoenix, USA), using a fluorinated SiO_2 cladding wrapping the Pr-doped core in order to guarantee the light guiding by the core-cladding interface.

Five samples were cut from different positions of the same preform. The first one was obtained as a slice of the Pr-doped bulk preform prior to drawing (Ø = 11 mm, thickness = 2.3 mm) and underwent a post-densification rapid thermal treatment at about 1500 - 1700 °C for 10 s. The second (Ø = 7 mm, thickness = 2 mm), the third (Ø = 4 mm, thickness = 1.1 mm) and the fourth (Ø = 1.4 mm, thickness = 0.9 mm) samples were cut from the residual of the fiber drawing process: in the following, they will be denoted as melted samples 1, 2, and 3 respectively. The last investigated sample was a piece of the fiber (Ø = 0.7 mm, thickness = 0.8 mm) fully drawn to the desired diameter: the five samples positions and their respective diameters are schematically shown in Fig. 1.

Photo-luminescence emission (PL) and excitation (PLE) steady-state spectra were performed with a homemade setup featuring a Xe-lamp coupled to a Jobin-Yvon Gemini 180 double monochromator as excitation source. The light emission was detected by a liquid nitrogen-cooled, back-illuminated and UV-enhanced, Jobin-Yvon Symphony charge-coupled device (CCD) detector coupled to a Jobin-Yvon Micro HR monochromator, equipped with a 150 grooves/mm grating and operating in the 200 – 1100 nm spectral range.

PL time decay measurements were carried out with a FLS980 Spectrometer (Edinburgh Instruments) featuring a pulsed light emitting diode (EPLED-250) with 920 ps pulse width as excitation source. The detector was a Hamamatsu R928P photomultiplier tube working in time-correlated single photon counting (TCSPC) mode.

The time response of the X-ray excited luminescence was measured using a custom-made pulsed X-ray system consisting of an ultrafast laser (200 fs pulses at 165 kHz), a light-excited X-ray tube, a Hamamatsu R3809U-50 microchannel PMT and an Ortec 9308 ps time analyzer. The impulse response of the system is 100 ps FWHM [25].

Radio-luminescence (RL) measurements were performed using a homemade apparatus featuring a liquid nitrogen-cooled, back-illuminated and UV-enhanced, CCD detector (Jobin-Yvon Spectrum One 3000) coupled to a monochromator (Jobin-Yvon Triax 180) with a 100 grooves/mm grating as detection system. RL excitation was obtained by X-ray irradiation through a beryllium window, using a Philips PW2274 X-ray diffraction tube with tungsten anode operated at 20 kV. At

this voltage, the X-rays generation mechanism exploits the *bremsstrahlung* process, leading to a characteristic continuous distribution energy spectrum. During the measurements, the sample area was limited to a disk with 2 mm diameter by an Al mask, to allow comparison between samples with different surface areas. The dose values reported in the text for X-ray irradiations were obtained by comparison with a calibrated $^{90}Sr–^{90}Y$ beta radioactive source and using optically stimulated luminescence emission from quartz crystalline powder (100-200 um). A dose rate of approximately 200 mGy/s was evaluated; such a dose rate, and consequently the hereafter reported dose values are to be considered as approximate, especially when compared with gamma irradiation doses.

The RL efficiency was defined, in an operative way, as the RL signal obtained by integrating the emitted light for 30s under irradiation. The dose delivered to the sample during this measurement was approximately 6 Gy. We employed such definition in order to evaluate the modification of the RL response as a function of the cumulated dose during prolonged irradiations; in Fig. 4 we report data normalized to the initial value.

All PL and RL emission spectra were corrected for the spectral response of the detection systems: the spectral response was obtained using an Oriel 63945 deuterium lamp and an Oriel 63358 quartz tungsten halogen lamp calibrated in the 250 – 2400 nm and 200 – 400 nm range respectively.

Wavelength-resolved thermally stimulated luminescence (WR-TSL) measurements were carried out using a homemade equipment. The heater section was custom designed and fabricated by Tecna s.r.l. and the heating rate was 1 °C/s. The detection system was the same one used for PL measurements.

Optical absorption (OA) spectra were acquired with a Varian Cary 50 Spectrophotometer and analyzed in terms of the minimum number of Gaussian components necessary to obtain a satisfactory spectrum reconstruction by using OriginPro 2015 software (Origin Lab. Corp.).
OA measurements were performed as a function of dose, recovery time, and annealing temperature. The samples were irradiated with a Machlett OEG50 therapy x-ray tube with tungsten anode, operated at 32 kV; in this case dose evaluation was performed by a PTW Duplex calibrated ionization chamber. The minimum delivered dose (D) was 1.3 Gy and then the successive irradiation steps were chosen in order to deliver to the samples 3 D, 10 D, 30 D, 100 D, 300 D and 1000 D, i.e. up to a final cumulated dose of 1300 Gy. At the end of the last irradiation step, OA spectra were acquired at various time intervals, without changing the sample position. The acquisition was performed repeatedly during the first five minutes, in order to verify the presence of fast decay processes. Afterwards, spectra were taken at intervals of one hour for a total cumulated time of about 20 hours, in order to monitor also the slower decay processes. A set of annealing cycles from 50 °C to 800 °C was eventually carried out. The samples were heated up, in 50 °C steps, holding them at each temperature for 15 minutes in a preheated oven. A few measurements

were also performed after gamma irradiation with a ^{60}Co source. In Section 3.3, both absorption spectra and radiation-induced ones are shown. The latter have been calculated as the differences between the spectra after irradiation and the spectrum before irradiation.

All measurements were performed at room temperature (RT).

3. Results and Discussion

3.1 Luminescence properties

RL and PL/PLE spectra are reported in Fig. 2 in order to put in evidence excitation and emission bands of Pr^{3+} ions inside the silica matrix. Two main groups of transitions can be identified in both RL and PL emission spectra: the broad composite 5d - 4f emission in the UV region and the 4f - 4f emission lines in the VIS - NIR region. The PLE spectrum of the 4f - 4f emissions clearly shows two excitation bands. The group of lines in the visible region can be attributed to transitions from the $^3H_4$ ground state level to the $^3P_0$, $^3P_1$ and $^3P_2$ levels. The main broad band peaking at about 5 eV (~ 250 nm) can be ascribed to the 4f - 5d transition [26]. This band characterizes also the PLE spectrum related to the 5d - 4f emission, although slightly shifted at higher energy and broadened. To better understand this behavior, further investigations have been performed on melted samples 1 and 2, and on the drawn fiber. The results are reported in Fig. S1. Interestingly, we observed (i) a high energy shift of both PLE spectra going from preform to fiber through melted samples; (ii) a systematic shift towards higher energy of the excitation of the 5d-4f transition with respect to that of the 4f-4f lines, which progressively reduces from preform to fiber. Concerning the former effect, it could be explained by crystal field modifications due to the fiber drawing. In fact, an analogous shift of the emission wavelength is also observed (from 298 nm in the preform to 284 nm in the fiber). The latter effect is more difficult to interpret. As a suggestion, we tentatively propose the interaction of Pr^{3+} energy levels with an optically active defect that is able to selectively excite in the short wavelength side the 5d-4f transition by non-radiative or radiative energy transfer, whose concentration is reduced by the drawing process; however this phenomenon deserves further investigations.

In Table 1 the emission lines energy values and the associated transitions observed in the emission spectra of Fig. 2 are reported, in accordance with previous results in the VIS – NIR [23, 24] and UV [12] regions. The emission lines are related mainly to transitions from the $^3P_0$ level to the various ^3H_j and ^3F_j sublevels. A higher resolution spectrum of the 4f - 4f emissions region is reported in Fig. S2 in the supporting information. The line broadening is intrinsic (due to inhomogeneous broadening) given that the instrumental resolution (1.3 nm at a wavelength of 600 nm) is lower than the full width at half maximum (FWHM) of the observed spectral structures. Referring to the Praseodymium energy level scheme of Fig. S3, the 5d levels are located below the $^1S_0$ 4f level in agreement with the observation of 5d - 4f transitions.

Pulsed scintillation (X-RL) and PL (λ_{exc} = 250 nm, λ_{em} = 295 nm) time decay measurements in the 2 μs time interval are reported together in Fig. 3 to allow their comparison. Distorted, not pure exponential decays are observed in both curves. The decays have been fitted in an operative way by the sum of exponential contributions. The PL decay is characterized by an initial fast component with 5 ns decay time and by a main contribution of about 35 ns. On the other hand, the scintillation decay features a faster part fitted with two components with 2.7 ns and 25 ns decay times, accompanied by a much slower contribution with about 160 ns decay time. The decay times and the relative intensities of all components are listed in Table 2. The initial decay distortions observed in both curves and approximated by the fit as very fast components are attributed to the presence of non-radiative recombinations and/or energy transfer processes. The contribution with 25-35 ns decay time is representative of the $5d_1$ - 4f transition of Pr^{3+}. The slow component, evidenced only in the scintillation decay and absent in PL, is attributed to the presence of defects temporarily trapping free electrons and then releasing the carriers with their characteristic emptying time.

3.2 RL hysteresis and TSL glow curves

The RL efficiency after prolonged irradiation, as described in Section 2, was also investigated in order to reveal the role of point defects (traps) as competitors with the luminescent recombination centers in free carrier capture during irradiation. The RL efficiency of all the samples was found to increase after prolonged exposure to ionizing radiation. The curves, normalized to their initial value, are shown in Fig. 4, where the relative intensity of the Pr^{3+} RL signal is plotted versus the cumulated absorbed dose during the irradiation with 20 keV (maximum energy) X-rays. The end of the irradiation sequence corresponds to a total cumulated dose of about 240 Gy. Each data point has been obtained by integrating the spectrum in the 240 – 945 nm range (this choice is justified by the fact that the spectral shape does not change during the measurements sequence). In all the cases, the intensity of the RL signal increased towards a saturation value. Comparing all samples and taking into account their respective positions (Fig. 1), it appears that such increase depends on the stage of the drawing process the sample derives from, and it becomes more pronounced as soon as the fiber condition is reached. In the field of scintillators, the increase of the light yield or RL signal in relation to irradiation history is known as hysteresis or “bright burn”. At first, the phenomenon of carrier trapping by localized defects competes with the radiative recombination, but, as the fraction of occupied traps progressively increases, the recombination process becomes more probable [27]. The phenomenon can have both a temporary and a permanent character, depending on the temporal stability of the involved traps. Shallow traps, which are emptied in a relatively short time and give rise to an afterglow or persistent luminescence signal, produce a temporary effect. On the other hand, if the traps are very deep and stable, no afterglow is observed, but their filling gives rise to a permanent increase of the RL efficiency. The enhancement of RL efficiency as a function of irradiation is a common characteristic of several scintillators and its

dose dependence might reflect the different concentrations, stabilities and capture cross-sections of carrier traps, as well as their spatial correlation with the recombination centers. This phenomenon has already been observed in several materials like, for instance, SiO_2:Tb [28], $Lu_2Si_2O_7$:Pr [27], YPO_4:Ce,Nd [29], SiO_2:Yb [30], and modeled [29, 31].

The right part of Fig. 4 shows the persistent luminescence measurements carried out after the irradiation end. All the samples exhibit a luminescence signal, originated by the detrapping process that becomes indistinguishable from the background level after some minutes. The luminescence curves do not follow a simple exponential decay. Such behavior is in agreement with the presence of several trap levels exhibiting also inhomogeneous broadening. Broad distributions of trap energy levels are commonly detected in glasses [32, 33]. Once more, comparing all samples and taking into account their positions (Fig. 1), a progressive acceleration of the decay is observed by getting closer to the fiber. This result is opposite to what observed for Yb-doped fibers [30]. In this respect, we remark that Pr ions capture holes during irradiation: therefore, their persistent luminescence is caused by the emptying of electron traps. The opposite occurs for Yb ions which capture electrons during irradiation, so their persistent luminescence is caused by the emptying of hole traps. Different kinds of traps display a different dependence upon the stage of the drawing process.

A deeper insight on trap levels has been pursued by WR-TSL measurements. The results obtained on all samples after X-rays irradiation are shown in Fig. 5. The glow curves related to the 5d - 4f emission (a) are characterized by a dominant peak at about 90 °C and by a lower peak at approximately 230 °C; similar peaks are detected in the glow curves related to the 4f – 4f emission (b), but with opposite relative intensities. The slight shift at higher temperature of the Pr-doped preform glow peaks is probably due to the difference in the sample thickness (2 mm) with respect to the other samples (~ 1 mm) causing a thermal lag during the sample heating. The different mutual intensity ratios of the TSL peaks obtained after integration on the 5d - 4f (a) and 4f - 4f (b) emissions might be related to a stronger thermal quenching of the 5d - 4f emission with respect to that of the 4f - 4f ones.

Similarly to what is observed for RL hysteresis and persistent luminescence, a dependence of the glow peak width on the stage of the drawing process can be clearly observed: the structures of the glow curves become better resolved, i.e. their width is significantly smaller, going from preform to fiber through melted samples. This feature can be ascribed to a readjustment of the silica matrix due to the heating process required by the fiber drawing, which influences the traps distribution and consequently the trap-related phenomena like RL hysteresis, persistent luminescence, and TSL. In this respect, we recall that previous Raman measurements performed in bulk sol-gel silica and fibers revealed that the intensities of D_1 and D_2 peaks due to symmetric stretching modes of fourfold and threefold rings of SiO_2 tetrahedra are higher in the fiber with respect to the bulk [34]. This is also in accordance with what observed on silica samples subjected to thermal treatments at

different temperatures, where the formation of fourfold and threefold rings of SiO_2 tetrahedra increased exponentially by temperature increasing [35].

3.3 OA and radiation hardness

The interaction of ionizing radiation with a scintillating material invariably creates radiation damage: this is a complicated process, which involves the host structure, its intrinsic defects as well as impurities, whose presence enhances the probability of creation of radiation-induced color centers. Therefore, the incident radiation can cause changes in the optical and scintillation properties of the material.

A photograph of a Pr-doped glass prior to irradiation is shown in Fig. 6 (a): the glass appears transparent and colorless. After exposure to 1 kGy X-ray irradiation, the sample got a brownish core, corresponding to the part where the luminescent activator is present (b).

The OA study was carried out only on SiO_2: 0.05 mol% Pr bulk preform and on the melted sample 1. Fig. 7 illustrates the OA spectra of SiO_2: 0.05 mol% Pr before and after X-ray irradiation, superimposed to the RL emission spectrum. In both OA spectra, the Pr^{3+} absorption lines from the $^3H_4$ ground state to the $^3P_2$, $^3P_1$ and $^3P_0$ excited states are fairly observed at 2.58, 2.64, and 2.75 eV, respectively. Strong absorption is also detected above 4.5 eV, likely related to the 4f - 5d transition of Pr^{3+} and possibly also to defect-related bands. In addition, after irradiation a broad absorption band becomes evident, overlapping with the fast 5d - 4f emission in the UV region (at about 4.0 eV). The UV light emitted by the RE luminescent centers can thus be likely re-absorbed by the material itself.

The radiation-induced absorption spectra obtained after X-ray irradiation as a function of increasing dose up to 1.3 kGy are reported in Fig. 8. A monotonic increase of the absorption is noted in both cases, without any significant shape modification. A significantly lower damage occurs in the melted sample with respect to the as-prepared preform, pointing towards a role of the fiber drawing process in the improvement of the radiation resistance of Pr-doped silica glass.

In Fig. 9, the numerical fit of the radiation-induced absorption spectrum in terms of Gaussian components is shown in order to put in evidence the presence of different induced absorption bands. A main broad band is clearly visible at about 3.3 eV accompanied by a weaker structure at about 2.3 eV, appearing as a shoulder on the main absorption peak. This feature is less pronounced in the melted sample with respect to the preform (whose spectrum and fit are reported in Fig. S4 in the supporting information). Again, this effect can be a consequence of the rearrangement of the matrix during the drawing process, leading to the removal of some defects, and it may deserve future additional investigations. The low energy band and the tail of the main induced absorption band, extending in the visible region, are responsible for the color appearing in the core of the sample after a high dose, as shown in Fig. 6 (b). At energies higher than 4.0 eV, the spectral shape suggests the presence of additional unresolved features. This high energy part

was taken into account by adding a third very broad component to the fit, which permits a satisfactory qualitative reconstruction of the experimental data. We recognize that, while the two lower energy bands are well defined, the parameters of the third one have poor physical meaning, because this energy region possibly contains even more than one band as well as scattering contributions. Table 3 lists the fit parameters only for the two well-identified components.

Considering that coloration mostly occurs in the Pr-doped core (see Fig. 6), we suggest that defects responsible for OA are likely related to the RE presence. In this respect, additional investigations should include samples with different Pr concentrations.

The evolutions of the OA spectra as a function of dose, RT recovery time and annealing temperature are reported in Fig. 10. Each data point corresponds to the amplitude of the corresponding Gaussian band. A monotonic increase of both bands as a function of dose is evidenced, with a tendency to saturation that is more pronounced for the 2.3 eV band (Fig. 10, panel a). During irradiation, both trap filling (resulting in color centers production) and emptying mechanisms coexist, yielding to a dose rate dependent transmission loss. The induced absorption reaches a saturation value when the rate of defect filling becomes equal to their emptying one. This mechanism is particularly evident for shallow defects characterized by relatively short decay times. A phenomenological model to describe the effect can be found in [36].

The induced defects responsible for the 2.3 and 3.3 eV bands are unstable and exhibit partial recovery at room temperature after irradiation. This spontaneous RT recovery is an important feature because it reduces the radiation damage effect without requiring any treatment on the sample, like thermal annealing or optical bleaching. This recovery can be caused by the spontaneous thermal escape of the carriers trapped in the absorbing center, or by their recombination with carriers of opposite sign freed from other unstable defects. The evolution of the OA spectra as a function of recovery time has been investigated for a total time of about 20 hours. The intensity of the induced absorption decreased monotonically; the transmission recovery turned out to be about 15 % for the main band peaking at 3.3 eV and much faster (about 45 %) for the lower energy component, as shown in panel (b) of Fig. 10.

As subsequent step, the glasses were treated with thermal annealing cycles up to 800 °C, to check the thermal release of charges from deeper traps responsible for color centers and the possibility of a complete recovery of the radiation damage. The samples were heated up, in steps of 50 °C, by holding them in a preheated oven for 15 minutes at each temperature step. By this procedure also charges in deep traps were released and a complete recovery was obtained after heat treatment at around 200 °C and at 600 °C for the 2.3 eV and for the 3.3 eV bands, respectively.

Finally, the melted sample 1 was irradiated also with a ^{60}Co γ source up to 1 kGy and the same spectral shape and structures were observed. The recovery rates after X-rays or γ exposure were found to be comparable, in spite of the different energy and rate of defect creation of the γ

radiation. In the future, we will extend this investigation by considering also the effect of electron beams in the GeV energy range on Pr-doped SiO_2 in fiber form.

4. Conclusions

The optical, scintillation and radiation hardness properties of Pr-doped sol-gel silica glass have been investigated in view of future applications in High Energy Physics experiments.

Optical absorption measurements after exposure to ionizing radiation reveal a high level of radiation damage, however a complete recovery occurs after thermal annealing cycles up to about 600 °C. An improvement in the radiation hardness, caused by a reduction of the concentration of defects acting as color centers under irradiation, is observed after fiber drawing. A link between this phenomenon and a readjustment of the Si-O network and of the traps distribution, induced by the high temperature treatment associated with the fiber drawing process, can be established. The changes induced in the material by the heating process can also be evidenced in the radio-luminescence hysteresis and thermo-luminescence glow curves.

The presented results help to increase the fundamental comprehension of the incorporation of Pr^{3+} ions in the SiO_2 matrix synthesized by sol-gel route and they could stimulate the improvement of synthesis techniques aimed at the control of material defectiveness.

To this purpose, future work should deeply focus on the investigation of RE-doped fibers properties in order to better disclose the factors contributing to enhance their radiation hardness.

Funding

This research was supported by the H2020 RISE Intelum Project (Grant Agreement 644260).

References

[1] A. Vedda, N. Chiodini, D. Di Martino, M. Fasoli, F. Morazzoni, F. Moretti, R. Scotti, G. Spinolo, A. Baraldi, R. Capelletti, M. Mazzera, M. Nikl, Insights into microstructural features governing Ce^{3+} luminescence efficiency in sol-gel silica glasses, Chem. Mater., 18 (2006) 6178-6185.

[2] F. Moretti, A. Vedda, N. Chiodini, M. Fasoli, A. Lauria, V. Jary, R. Kucerkova, E. Mihokova, A. Nale, M. Nikl, Incorporation of Ce^{3+} in crystalline Gd-silicate nanoclusters formed in silica, J. Lumin., 132 (2012) 461-466.

[3] A. Vedda, N. Chiodini, M. Fasoli, A. Lauria, F. Moretti, D. Di Martino, A. Baraldi, E. Buffagni, R. Capelletti, M. Mazzera, P. Bohacek, E. Mihokova, Evidences of rare-earth nanophases embedded in silica using vibrational spectroscopy, IEEE Trans. Nucl. Sci., 57 (2010) 1361-1369.

[4] I. Veronese, C.D. Mattia, M. Fasoli, N. Chiodini, E. Mones, M.C. Cantone, A. Vedda, Infrared luminescence for real time ionizing radiation detection, Appl. Phys. Lett., 105 (2014).
[5] R. Becker, G. Dissertori, A. Gendotti, Q. Huang, D. Luckey, W. Lustermann, S. Lutterer, F. Nessi-Tedaldi, F. Pandolfi, F. Pauss, M. Peruzzi, M. Quittnat, R. Walny, Proof-of-principle of a new geometry for sampling calorimetry using inorganic scintillatori plates, J. Phys.: Conf. Series, 587 (2015) 012039
[6] A. Penzo, Y. Onel, The CMS-HF quartz fiber calorimeters, J. Phys.: Conf. Series, 160 (2009).
[7] A. Benaglia, M. Lucchini, K, Pauwels, C. Tully, T. Medvedeva, A. Heering, C. Dujardin, V. Kononets, K. Lebbou, N. Aubry, S. Faraj, G. Ferro, P. Lecoq, E. Auffray, Test beam results of a high granularity LuAG fibre calorimeter prototype, J. Inst., 11 (2016) P05004
[8] M. Lucchini, T. Medvedeva, K. Pauwels, C. Tully, A. Heering, C. Dujardin, K. Lebbou, P. Lecoq, E. Auffray, Test beam results with LuAG fibers for next-generation calorimeters, J. Inst, 8 (2013) P10017
[9] M. Cascella, S. Franchino, S. Lee, Fiber and Crystals Dual Readout calorimeters, Int. J. Mod. Phys. A (2016), arXiv:1611.03627v2
[10] K. Pauwels, C. Dujardin, S. Gundacker, K. Lebbou, P. Lecoq, M. Lucchini, F. Moretti, A. G. Petrosyan, X. Xu, E. Auffray, Single crystalline LuAG fibers for homogeneous dual-readout calorimeters, J. Inst, 8 (2013) P09019
[11] CMS Collaboration, Technical Proposal for the Phase II Upgrade of the Compact Muon Solenoid, CERN-LHCC-2015-010 (2015) LHCC-P-008
[12] Y. Sun, M. Koshimizu, S. Kishimoto, Synthesis and characterization of Pr^{3+}-doped glass scintillators prepared by the sol-gel method, J. Sol-Gel Sci. Technol., 62 (2012) 313-318.
[13] S. David, C. Michail, I. Seferis, I. Valais, G. Fountos, P. Liaparinos, I. Kandarakis, N. Kalyvas, Evaluation of Gd_2O_2S:Pr granular phosphor properties for X-ray mammography imaging, J. Lumin. 169 (2016) 706-710
[14] H. Ogino, A. Yoshikawa, M. Nikl, A. Krasnikov, K. Kamada, T. Fukuda, Growth and scintillation properties of Pr-doped $Lu_3Al_5O_{12}$ crystals, J. Cryst. Growth, 287 (2006) 335-338.
[15] W. Drozdowski, P. Dorenbos, J. de Haas, R. Drozdowska, A. Owens, K. Kamada, K. Tsutsumi, Y. Usuki, T. Yanagida, A. Yoshikawa, Scintillation Properties of Praseodymium Activated $Lu_3Al_5O_{12}$ Single Crystals, IEEE Trans. Nucl. Sci., 55 (2008) 2420.
[16] T. Yanagida, Y. Fujimoto, K. Kamada, D. Totsuka, H. Yagi, T. Yanagitani, Y. Futami, S. Yanagida, S. Kurosawa, Y. Yokota, A. Yoshikawa, M. Nikl, Scintillation properties of transparent ceramic Pr:LuAG for different Pr concentration, IEEE Trans. Nucl. Sci., 59 (2012) 2146-2151.
[17] G. Mares, M. Nikl, A. Beitlerova, P. Horodysky, K. Blazek, K. Bartos, C. D'Ambrosio, Scintillation Properties of Ce^{3+}- and Pr^{3+}-Doped LuAG, YAG and Mixed $Lu_xY_{1-x}AG$ Garnet Crystals, IEEE Trans. Nucl. Sci., 59 (2012) 2120.

[18] M. Nikl, J. Pejchal, E. Mihokova, J.A. Mares, H. Ogino, A. Yoshikawa, T. Fukuda, A. Vedda, C. D'Ambrosio, Antisite defect-free $Lu_3(Ga_xAl_{1-x})_5O_{12}$:Pr scintillator,, Appl. Phys. Lett., 88 (2006) 141916.
[19] K. Kamada, T. Yanagida, J. Pejchal, M. Nikl, T. Endo, K. Tsutsumi, Y. Fujimoto, A. Fukabori, A. Yoshikawa, Improvement of Scintillation Properties in Pr Doped $Lu_3Al_5O_{12}$ Scintillator by Ga and Y Substitutions, IEEE Trans. Nucl. Sci., 59 (2012) 2130.
[20] M. Zhuravleva, A. Novoselov, E. Mihokova, J.A. Mares, A. Vedda, M. Nikl, A. Yoshikawa, Crystal growth and scintillating properties of (Pr,Si)-doped $YAlO_3$, Cryst. Res. Technol., 42 (2007) 1324-1328.
[21] M. Nikl, J.A. Mares, A. Vedda, M. Fasoli, V. Laguta, E. Mihokova, J. Pejchal, M. Zhuravleva, A. Yoshikawa, K. Nejezchleb, Can Pr-doped YAP scintillator perform better?, IEEE Trans. Nucl. Sci., 57 (2010) 1168-1174.
[22] A. Novoselov, H. Ogino, A. Yoshikawa, M. Nikl, J. Pejchal, J.A. Mares, A. Beitlerova, C. D'Ambrosio, T. Fukuda, Study on crystal growth and luminescence properties of Pr-doped RE_2SiO_5 (RE=Y, Lu), J. Cryst. Growth, 287 (2006) 309-312.
[23] W. Strçk, J. Legendziewicz, E. Łukowiak, K. Maruszewski, J. Sokolnicki, A.A. Boiko, M. Borzechowska, Optical properties of Pr^{3+} doped silica gel glasses obtained by sol-gel method, Spectrochim. Acta, Part A, 54 (1998) 2215-2221.
[24] R. Percival, M. Phillips, D. Hanna, Characterization of spontaneous and stimulated emission from Prasodymium (Pr^{3+}) ions doped into a silica-based monomode optical fiber, IEEE J. Quantum Electron., 25 (1989) 2119.
[25] S. Derenzo, G. Bizarri, R. Borade, E. Bourret-Courchesne, R. Boutchko, A. Canning, A. Chaudhry, Y. Eagleman, G. Gundiah, S. Hanrahan, M. Janecek, M. Weber, New scintillators discovered by high-throughput screening, Nucl. Instrum. Methods Phys. Res., Sect. A, 652 (2011) 247-250.
[26] Y. Shen, X. Feng, Y. Shi, A. Vedda, F. Moretti, C. Hu, S. Liu, Y. Pan, H. Kou, L. Wu, The radiation hardness of Pr:LuAG scintillating ceramics, Ceram. Int., 40 (2014) 3715-3719.
[27] E. Dell'Orto, M. Fasoli, G. Ren, A. Vedda, Defect-driven radioluminescence sensitization in scintillators: The case of $Lu_2Si_2O_7$:Pr, J. Phys. Chem. C, 117 (2013) 20201-20208.
[28] M. Fasoli, N. Chiodini, A. Lauria, F. Moretti, A. Vedda, Effect of deep traps on the optical properties of Tb^{3+} doped sol-gel silica, Phys. Status Solidi C, 4 (2007) 1056-1059.
[29] F. Moretti, G. Patton, A. Belsky, M. Fasoli, A. Vedda, M. Trevisani, M. Bettinelli, C. Dujardin, Radioluminescence sensitization in scintillators and phosphors: Trap engineering and modeling, J. Phys. Chem. C, 118 (2014) 9670-9676.
[30] I. Veronese, C. De Mattia, M. Fasoli, N. Chiodini, M.C. Cantone, F. Moretti, C. Dujardin, A. Vedda, Role of Optical Fiber Drawing in Radioluminescence Hysteresis of Yb-Doped Silica, J. Phys. Chem. C, 119 (2015) 15572-15578.

[31] F. Moretti, G. Patton, A. Belsky, A.G. Petrosyan, C. Dujardin, Deep traps can reduce memory effects of shallower ones in scintillators, PCCP, 18 (2016) 1178-1184.
[32] A. Vedda, N. Chiodini, D. Di Martino, M. Fasoli, L. Griguta, F. Moretti, E. Rosetta, Thermally stimulated luminescence of Ce and Tb doped SiO_2 sol-gel glasses, J. Non-Cryst. Solids, 351 (2005) 3699-3703.
[33] I. Veronese, M. Fasoli, M. Martini, F. Moretti, A. Vedda, G. Loi, E. Mones, Phosphorescence of SiO_2 optical fibres doped with Ce^{3+} ions, Phys. Status Solidi C, 4 (2007) 1024-1027.
[34] A. Vedda, N. Chiodini, D. Di Martino, M. Fasoli, S. Keffer, A. Lauria, M. Martini, F. Moretti, G. Spinolo, M. Nikl, N. Solovieva, G. Brambilla, Ce^{3+}-doped fibers for remote radiation dosimetry, Appl. Phys. Lett., 85 (2004) 6356-6358.
[35] A.E. Geissberger, F.L. Galeener, Raman studies of vitreous SiO_2 versus fictive temperature, Phys. Rev. B, 28 (1983) 3266-3271.
[36] L. Zhang, D. Bailleux, A. Bornheim, K. Zhu, R.Y. Zhu, Performance of the monitoring light source for the CMS lead tungstate crystal calorimeter, IEEE Trans. Nucl. Sci., 52 (2005) 1123-1130.

Figure captions

Fig. 1: Schematic sketch of the final part of a drawn preform. The five samples investigated, marked by arrows, were taken as representative of different stages of the preform drawing process. Their diameters are also reported in the figure.

Fig. 2: Comparison between (a) RL and (b) PL emission spectra (λ_{exc} = 255 – 260 nm) of SiO_2: 0.05% Pr preform normalized to the 4f – 4f emissions performed with a 100 grooves/mm and 150 grooves/mm grating respectively. (c) and (d) PL excitation spectra taken integrating the emission in the 580 – 670 nm and 305 – 330 nm range respectively. Measurements carried out on the other samples led to comparable results.

Fig. 3: (a) PL decay (λ_{exc} = 250 nm, λ_{em} = 295 nm) and (b) spectrally unresolved scintillation decay (pulsed X-rays source) of Pr^{3+} luminescence. Red lines: exponential fit to the experimental data. The deconvolution of the PL decay signal with the PL pulse has been carried out. Data were normalized to their initial value. PL and scintillation decay measurements were performed on the SiO_2: 0.05% Pr preform sample.

Fig. 4: (a) Room temperature RL efficiency of SiO_2: 0.05% Pr versus irradiation dose and time, for a total cumulated dose of 240 Gy. Each data point has been obtained by integrating the RL spectrum in the 240 – 945 nm range. Data are normalized to the initial value. (b) After the irradiation stops, a persistent luminescence signal is detected as a function of time. In the inset, an enlargement of the persistent luminescence decays is reported.

Fig. 5: TSL glow curves of bulk SiO_2:0.05% Pr and fiber obtained after 500 Gy X-rays irradiation at RT. A heating rate of 1 °C/s was adopted. The curves were obtained by integration of wavelength resolved TSL measurements from 270 to 370 nm (a) and from 570 to 670 nm (b) to independently investigate the temperature dependence of the two main Pr^{3+} emissions. The curves are normalized to their maximum values.

Fig. 6: (a) Picture of the SiO_2: 0.05% Pr melted sample 1 before irradiation and (b) after 1 kGy irradiation. The size of the glass sample was approximately 7 mm in diameter and 2 mm in thickness.

Fig. 7: Solid lines: optical absorption spectra of SiO_2: 0.05% Pr preform before and after 1 kGy X-ray irradiation. Dashed line: RL emission spectrum under 20 kV X-ray excitation. Measurements carried out on the melted sample 1 led to comparable results.

Fig. 8: Radiation-induced optical absorption spectra of (a) SiO_2: 0.05% Pr preform and (b) SiO_2: 0.05% Pr melted sample 1 as a function of increasing dose. In the melted sample 1, the induced absorption coefficient is significantly lower.

Fig. 9: Numerical fit (red solid line) of the radiation-induced optical absorption spectrum of SiO_2: 0.05% Pr melted sample 1 after 1 kGy irradiation, carried out as a sum of three Gaussian components (black dashed lines).

Fig. 10: Radiation-induced absorption coefficient of SiO_2: 0.05% Pr preform as a function of (a) dose, (b) room temperature recovery time and (c) annealing temperature. The behavior of the two main Gaussian components is reported. The ordinate scales are the same in the three panels. Dashed lines are guides for the eyes. Measurements carried out on the melted sample 1 led to comparable results and are not reported.

Tables

	Transition	Wavelength (nm)	Energy (eV)
4f – 4f	$^1D_2 \rightarrow {}^3F_2$	894 ± 4	1.38 ± 0.01
	$^1D_2 \rightarrow {}^3H_6$	868 ± 4	1.43 ± 0.01
	$^3P_0 \rightarrow {}^3F_4$	747 ± 3	1.66 ± 0.01
	$^1D_2 \rightarrow {}^3H_5$	708 ± 3	1.75 ± 0.01
	$^3P_0 \rightarrow {}^3F_2$	657 ± 3	1.89 ± 0.01
	$^3P_0 \rightarrow {}^3H_6$	635 ± 3	1.95 ± 0.01
	$^1D_2 \rightarrow {}^3H_4$	616 ± 3	2.01 ± 0.01
	$^3P_0 \rightarrow {}^3H_5$	543 ± 3	2.28 ± 0.01
	$^3P_0 \rightarrow {}^3H_4$	487 ± 3	2.55 ± 0.01
5d – 4f	$5d_1 \rightarrow {}^3H_6$	354 ± 2	3.50 ± 0.01
	$5d_1 \rightarrow {}^3H_4$	295 ± 2	4.20 ± 0.02

Table 1: Spectral positions of the Pr^{3+} transitions in SiO_2 matrix observable in the RL and PL emission spectra of Fig.2. For a more detailed illustration of the above-mentioned transitions in the 4f – 4f region, refer to Fig. S2 in the supporting information.

	τ_1 (ns)	τ_2 (ns)	τ_3 (ns)
Pulsed X-RL	2.7 (10%)	24 (40%)	160 (50%)
PL Decay	5 (30%)	35 (70%)	

Table 2: Decay times of the 295 nm PL emission and of the scintillation emission of Pr^{3+}ions obtained from the three-exponential approximation $I(t) = \sum_i A_i \tau_i + background$ in SiO_2:0.05% Pr preform. In parenthesis the relative intensities of the decay components are reported.

	First Component	Second Component
Amplitude (cm^{-1})	0.2	2.2
Energy (eV)	2.3	3.3
FWHM (eV)	0.6	1.4

Table 3: Fit parameters (amplitudes, peak energies and full widths at half-maximum - *FWHM*) of the two main Gaussian components of Fig. 9. An uncertainty of ± 0.5 eV is estimated for the energy values, taking into account the standard error resulting from the numerical fit and the uncertainties associated with the fit procedure itself.

Optical characterization and influence of the fiber drawing process in the radiation hardness of Pr-doped Sol-Gel silica glasses

Francesca Cova[a], Mauro Fasoli[a] *, Federico Moretti[a], Norberto Chiodini[a], Kristof Pauwels[b], Etiennette Auffray[c], Marco Toliman Lucchini[c], Edith Bourret[d], Ivan Veronese[e,f], Eduardo d'Ippolito[e], Anna Vedda[a]

[a] Department of Materials Science, University of Milano-Bicocca, Via Cozzi 55, 20125 Milano (Italy)
[b] Department of Physics, University of Milano-Bicocca, Piazza della Scienza 3, 20125 Milano (Italy)
[c] CERN, Route de Meyrin, 1211 Geneva 23 (Switzerland)
[d] Materials Science Division, Lawrence Berkeley National Laboratory, Berkeley, CA (USA)
[e] Department of Physics, University of Milano, Via Celoria 16, 20133 Milano (Italy)
[f] INFN, Unit of Milano, Via Celoria 16, 20133 Milano (Italy)

* Corresponding author at: Department of Materials Science, University of Milano-Bicocca, Via Cozzi 55, 20125 Milano (Italy)
E-mail address: mauro.fasoli@mater.unimib.it (Mauro Fasoli)

SUPPORTING INFORMATION

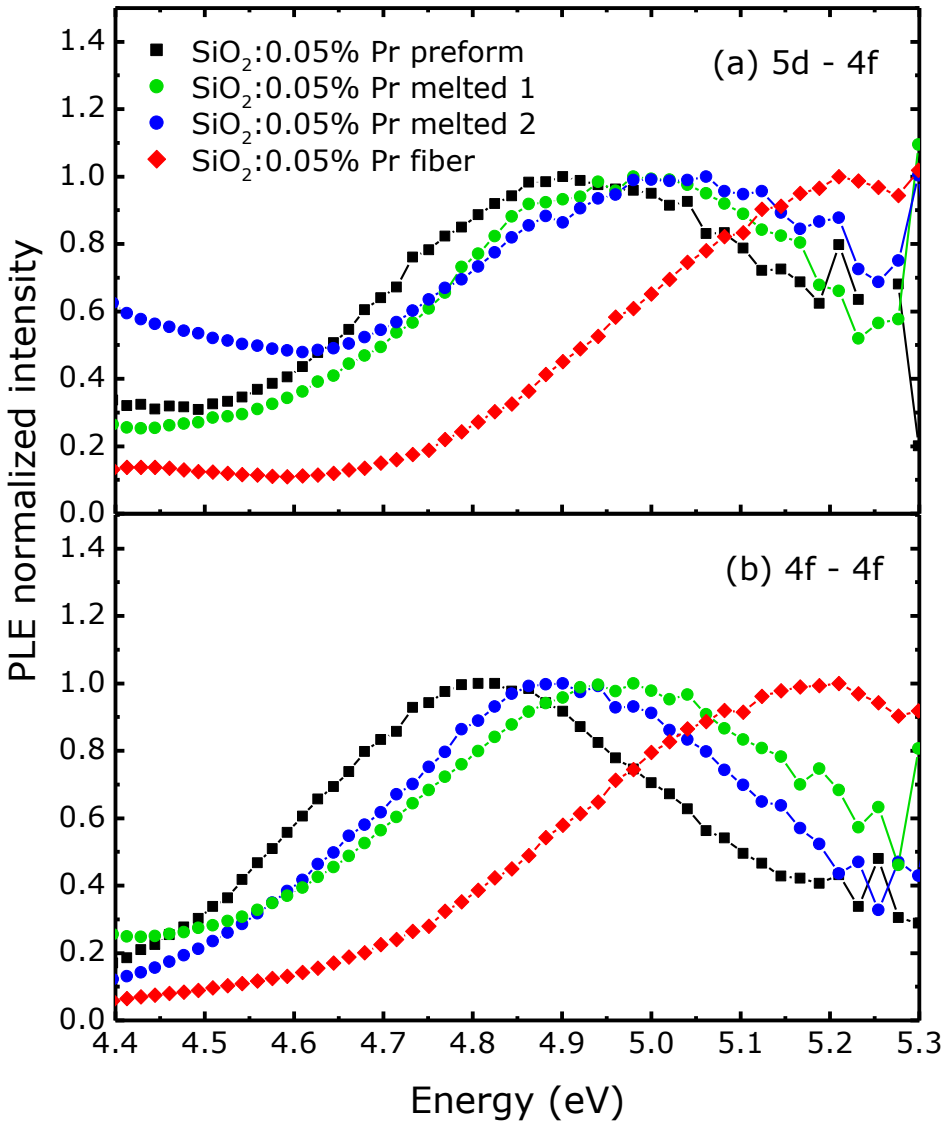

Fig. S1: PLE spectra of SiO_2:0.05% Pr (a) in the 5d – 4f emission region (λ_{em} = 290 – 350 nm) and (b) in the 4f – 4f emission region (λ_{em} = 580 – 670 nm).

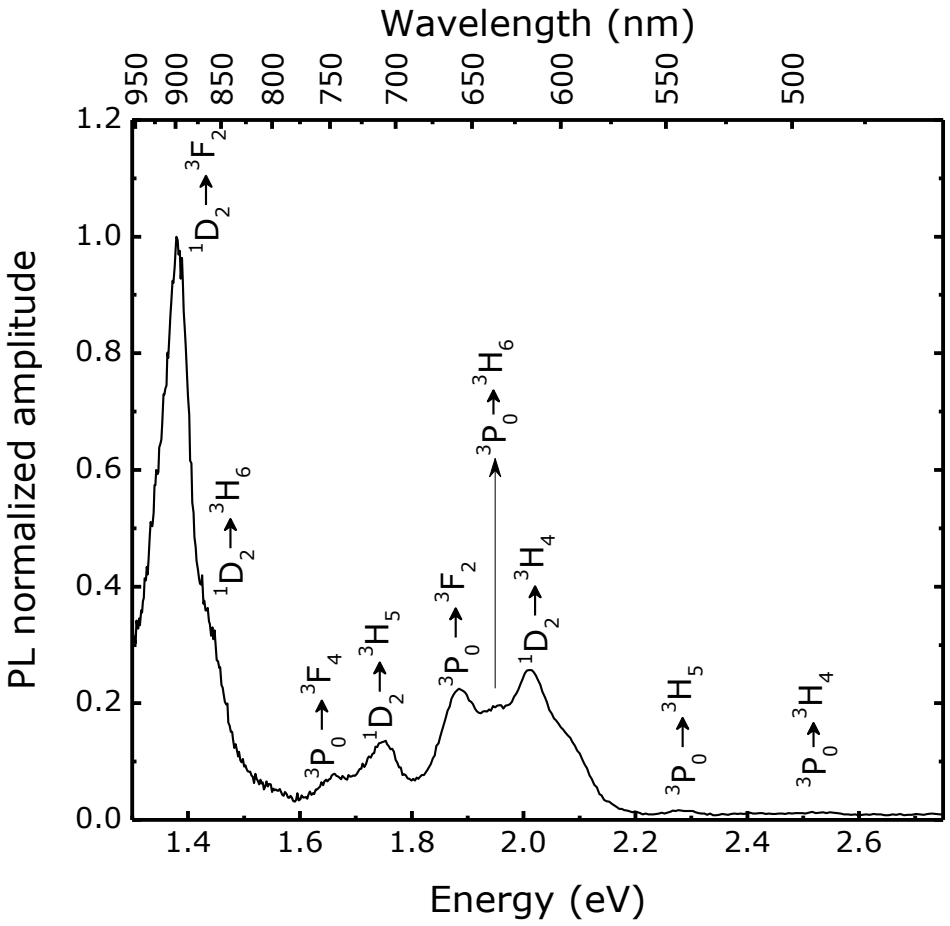

Fig. S2: PL emission spectrum (λ_{exc} = 245 – 300 nm) of SiO_2:0.05% Pr in the 4f – 4f region. The transitions associated with the observable emission lines are also reported. Refer to Table 1 for a complete list of the transition energies.

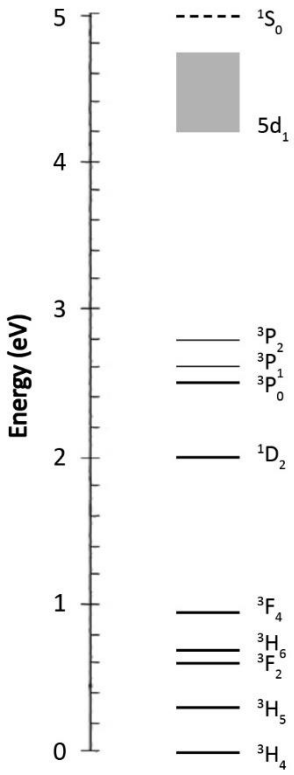

Fig. S3: Energy levels of the *4f*^{n}*5d* configurations of the Pr^{3+} ion embedded in the SiO_2 matrix.

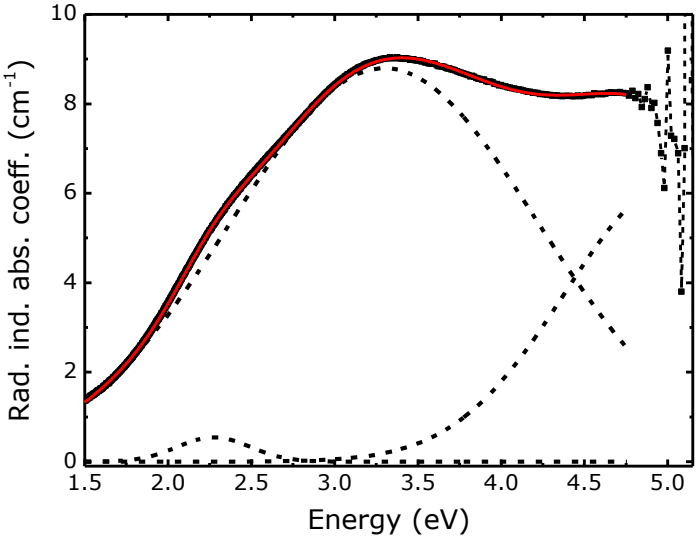

Fig. S4: Numerical fit (red solid line) of the induced optical absorption spectrum of SiO_2: 0.05% Pr preform after 1 kGy irradiation, carried out as a sum of three Gaussian components (black dashed lines).